Hollow Mesoporous Silica Nanoparticles Gated by Chitosan-Copper Sulfide Composites as Theranostic Agents for the Treatment of Breast Cancer

Shiwei Niu[a,b†], Xuejing Zhang[a†], Gareth R. Williams[c], Jianrong Wu[a], Feng Gao[d], Zi Fu[a], Xia Chen[a], Sheng Lu[e*], Li-Min Zhu[a*]

[a] College of Chemistry, Chemical Engineering and Biotechnology, Donghua University, Shanghai 201620, P.R. China;

[b] Yunnan Key Laboratory of Stem Cell and Regenerative Medicine, Science and Technology Achievement Incubation Center, Kunming Medical University, Kunming 650500, P.R. China

[c] UCL School of Pharmacy, University College London, 29-39 Brunswick Square, London, WC1N 1AX, UK

[d] Department of Ultrasound, Shanghai General Hospital, Shanghai Jiaotong University School of Medicine, Shanghai 201600, P.R. China

[e] Yunnan Key Laboratory of Digital Orthopaedics, Department of Orthopaedics, the First People's Hospital of Yunnan Province, Kunming 650500, P.R. China

[†] Co-first authors, contributed equally to this work.

[*] Corresponding authors at: College of Chemistry, Chemical Engineering and Biotechnology, Donghua University, Shanghai 201620, PR China (L.-M. Zhu) and Yunnan Key Laboratory of Digital Orthopaedics, Department of Orthopaedics, the First People's Hospital of Yunnan Province, Kunming 650500, PR China (S. Lu).

E-mail addresses: lzhu@dhu.edu.cn (L.-M. Zhu), drlusheng@163.com (S. Lu).

ABSTRACT

The combination of chemotherapy and photothermal therapy (PTT) into a single formulation has attracted increasing attention as a strategy for enhancing cancer treatment. Here, hollow mesoporous silica nanoparticles (HMSNs) were used as a base carrier material, loaded with the anti-cancer drug doxorubicin (DOX), and surface functionalized with chitosan (CS) and copper sulfide (CuS) nanodots to give HMSNs-CS-DOX@CuS. In this formulation, the CuS dots act as gatekeepers to seal the surface pores of the HMSNs, preventing a burst release of DOX into the systemic circulation. S-S bonds connect the CuS dots to the HMSNs; these are selectively cleaved under the reducing microenvironment of the tumor, permitting targeted drug release. This, coupled with the PTT properties of CuS, results in a potent chemo/PTT platform. The HMSNs-CS-DOX@CuS nanoparticles have a uniform size (150 ± 13 nm), potent photothermal properties (η= 36.4 %), and tumor-targeted and near infrared (NIR) laser irradiation-triggered DOX release. *In vitro* and *in vivo* experimental results confirmed that the material has good biocompatibility, but is effectively taken up by cancer cells. Moreover, the CuS nanodots permit, simultaneous thermal/photoacoustic dual-modality imaging. Treatment with HMSNs-CS-DOX@CuS and NIR irradiation caused extensive apoptosis in cancer cells both *in vitro* and *in vivo*, and could dramatically extend the lifetimes of animals in a murine breast cancer model. The system developed in this work therefore merits further investigation as a potential nanotheranostic platform for cancer treatment.

Keywords: Combination therapy; Hollow mesoporous silica nanoparticles; Copper sulfide; Photoacoustic imaging; Nanotheranostic

1. Introduction

Cancer is the second leading cause of mortality worldwide, and breast cancer in particular poses a serious threat to women's health [1]. The incidence of cancer is expected to continue to increase over the next 20 years, despite the fact that extensive efforts have been devoted to cancer research [2], and thus the search for new treatments continues. It is well known that conventional cancer chemotherapy is accompanied by unavoidable off-target toxicity, and combination therapies which can ameliorate these issues are attracting significant attention. Much effort has been made to construct composite nanoparticles (NPs) for combined chemotherapy and

photothermal therapy (chemo-PTT) platforms [3-5].

PTT has emerged as an adjuvant therapy of choice because it has high therapeutic efficiency, is non-invasive, permits deep tissue penetration, and has only minor side effects [3, 6]. PTT converts near-infrared light (NIR) energy into heat, which is then used to kill cancer cells. To do this effectively, PTT agents with high photothermal conversion efficiency and good biocompatibility are required to convert NIR into heat [7, 8]. There are many such materials available, including carbon nanomaterials, copper chalcogenides, and gold NPs [9, 10]. Among these, copper sulfide (CuS) in particular has been widely explored by dint of its simple preparation process, low cytotoxicity, and high photothermal conversion efficiency. Moreover, ultrasmall CuS NPs are well-known for strong absorbance in the NIR region [11-14].

To achieve combined chemotherapy and PTT, CuS and anticancer drugs can be incorporated into the same platform. The heating effect of PTT can then promote drug release as well as ablating tumors *via* local heating, leading to synergistic therapy. One suitable nanoplatform is based on hollow mesoporous silica nanoparticles (HMSNs), which have been explored extensively because of their large surface area, adjustable pore volume and size, and potential for surface modification [15, 16]. The central hollow cavity in HMSNs confers them with relatively high drug loading capacities [17, 18]. However, the presence of pores on the surface of HMSNs tends to lead to rapid drug release. A “gatekeeper” is required to seal these surface pores and realize targeted drug delivery [19, 20]. We hypothesized here that CuS could be combined with HMSNs to act as both gatekeeper and PTT agent. In this way, the incorporation of CuS would both confer the nanocomposite with PTT capacity, and also help to control drug release. It could further endow the nanoplatform with theranostic capabilities, as CuS is a typical p-type semiconductor material and in addition to its therapeutic potential can be used as a photoacoustic (PA) contrast agent and NIR thermal imaging agent [21]. CuS also has low biotoxicity, and is easily excreted from the body, both of which are highly promising for clinical translation [22].

HMSN particle sizes are highly controllable, and by ensuring they possess an appropriate size scientists can achieve passive targeting to a tumor *via* the enhanced permeability and retention (EPR) effect [23]. This in turn can ensure localized drug release and increase therapeutic efficacy while reducing side effects [24, 25]. The microenvironment of the tumor tissue is very different from that of normal healthy tissue (e.g. in terms of pH, reducing environment, and temperature),

meaning it is possible to conceive of the construction of a stimulus-responsive drug delivery system based on HMSNs [26-28].

In this work, chitosan (CS) was modified with thioglycolic acid to give CS-SH, and then covalently bonded onto HMSNs by disulfide linkage. CS is well established as a suitable material for use in drug delivery systems: it is widely available, low-cost, biodegradable, biocompatible, and pH-sensitive [29-32]. CS can hence be used to improve the biocompatibility and solubility of a material. Here, the anticancer drug doxorubicin (DOX) was encapsulated in the central cavity of the CS-modified HMSNs and the unreacted sulfhydryl groups on CS used to bind to CuS through disulfide bonds. This results in CuS nanodots capping the pore on the surface of the HMSNs (giving HMSNs-CS-DOX@CuS NPs). It is well known that disulfide (S-S) bonds show reduction-responsive behavior and can be cleaved in the presence of reducing agents such as glutathione (GSH). GSH levels in cancer cells are several times higher than that in normal cells [33-35], and thus once the HMSNs-CS-DOX@CuS system reaches the tumor the S-S bonds linking the CuS NPs to the particle surface can be expected to break. If NIR irradiation is also applied, then the PTT heating mediated by CuS will accelerate this effect. This will cause DOX to be released, and induce cancer cell apoptosis. The strong NIR absorption of CuS further allows thermal and PA imaging to be undertaken, thus endowing the system with theranostic potential. This strategy of this work is illustrated in Scheme 1.

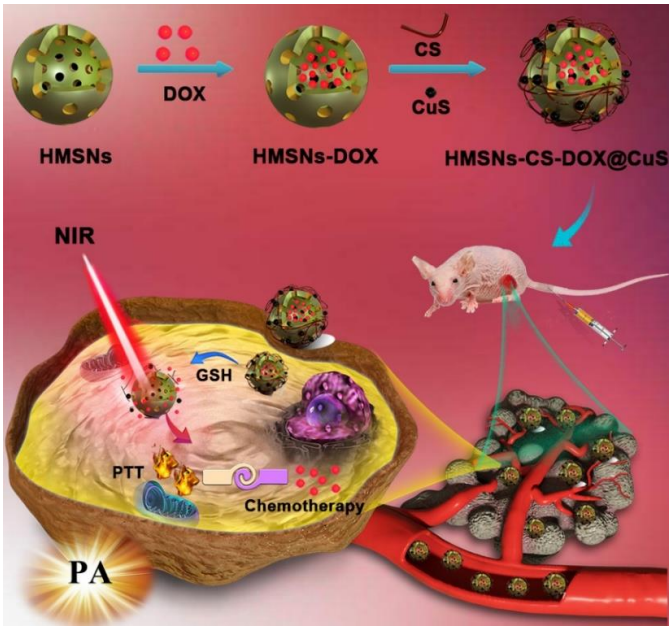

Scheme 1. Schematic illustration of the concept behind using HMSNs-CS-DOX@CuS for thermal-PA imaging guided tumor chemo-PTT therapy.

2. Materials and methods

2.1. Materials

Tetraethyl orthosilicate (TEOS), γ-mercaptopropyltriethoxysilane (MPTMS), *n*-octadecyltrimethoxysilane (C_{18}TMS), thioglycolic acid and doxorubicin hydrochloride (DOX·HCl) were purchased from the Aladdin Company (Shanghai, China). 3-(4,5-dimethyl-thiazol-yl)-2,5-diphenyltetrazolium bromide (MTT), 1-(3-dimethylaminopropyl)-3-ethylcarbodiimide hydrochloride (EDC·HCl), *N'*-hydroxysuccinamide (NHS), *N, N'*-dimethylformamide (DMF), and calcein-AM and propidium iodide (PI) were sourced from Sigma-Aldrich (St. Louis, MO, USA). Chitosan (CS) was obtained from Weikang Biotechnology Co. Ltd (Linyi, China). Cupric chloride ($CuCl_2 \cdot 2H_2O$) and sodium sulfide ($Na_2S \cdot 9H_2O$) were purchased from the Beijing Chemical Reagent Co Ltd (Beijing, China). DIR (1,10-dioctadecyl-3,3,30,30-tetramethylindotricarbo cyanine iodide) came from Biotium (Fremont, CA, USA). 4',6-diamidino-2-phenylindole (DAPI) was obtained from the Dingguochangsheng Biotechnology Co. Ltd. (Beijing, China). Hematoxylin and eosin (H&E), Annexin V FITC/PI (propidium iodide), and terminal deoxynucleotidyl transferase-mediated dUTP nick-end labeling (TUNEL) detection kits were provided by Beyotime Biotechnology (Shanghai, China). Dialysis bags (molecular weight cutoff of 3500 Da) were purchased from Yuanye Biotechnology Co. Ltd (Shanghai, China). MilliQ water (resistivity > 18.2 MΩ cm^{-1}) was generated using a MilliQ academic water purification system (Millipore, Burlington, MA, USA). All other chemicals and solvents used were of at least analytical grade.

HUVEC and MDA-MB-231 cells were purchased from the Type Culture Collection of the Chinese Academy of Sciences (Shanghai, China). Dulbecco's Modified Eagle Medium (DMEM), fetal bovine serum (FBS), penicillin, streptomycin and trypsin-EDTA were procured from Gibco (Carlsbad, CA, USA).

Female nude mice (18-20 g, 5-6 weeks old) and male Sprague-Dawley (SD) rats (200-220 g, 5-6 weeks old) were supplied by the Animal Center of Kunming Medical University (Kunming, China) and housed under specific pathogen-free conditions at 20-22 ℃. All animal care and handling procedures were conducted in accordance with the Guide for the Care and Use of Laboratory Animals published by the US National Institutes of Health (NIH Publication No. 8523, revised 1985). The experimental protocols were reviewed and approved by the Animal Care and

Use Committee of Kunming Medical University (ref: KMMU 2015002).

2.2. Synthesis of HMSNs-CS-DOX@CuS

Preparation of HMSNs. Anhydrous ethanol (71.4 mL), ultrapure water (10 mL), and $NH_3 \cdot H_2O$ (3.14 mL) were mixed in a round-bottomed flask. Under magnetic stirring, the solution was maintained at 30 °C for 20 min before 6 mL of TEOS was added, and stirring then continued for 1 h to obtain solid silica nanoparticles ($sSiO_2$). A mixture of TEOS (5 mL) and $C_{18}TMS$ (2 mL) was next added rapidly and magnetic stirring continued for a further 1 h. The product was collected by centrifugation and transferred into a mixture of anhydrous ethanol and hydrochloric acid (40 % 10/1 v/v, 50 mL). The resultant mixture was stirred at 80 °C for 12 h. After centrifugation, the product was dispersed in 40 mL of an aqueous 0.6 M Na_2CO_3 solution under magnetic at 80 °C for 6 h. Afterwards, the product was collected by centrifugation and washed with water three times. Finally, the products were dried at 100 °C and calcined at 550 °C for 6 h to obtain HMSNs (for the synthetic route sees Scheme S1).

Preparation of HMSNs-SH and CS-SH. The aggregated particles were removed and the well-dispersed HMSNs particles were used for further functionalization. HMSNs (100 mg) were dispersed in isopropyl alcohol (120 mL) with an ultrasonic treatment, and 120 mL MPTMS added dropwise. The mixture was stirred under nitrogen for 24 h to obtain HMSNs-SH. CS was completely dissolved in DMF solution (1 g CS in 100 mL of DMF with 1.0 % v/v aqueous acetic acid) prior to thioglycolic acid (0.34 g) being added. Reaction was allowed to proceed for 12 hours in the presence of NHS (104 mg) and EDC (68 mg); this mixed solution was then subjected to dialysis (MWCO=3500 Da) for 72 h against deionized water to give CS-SH.

DOX loading and CuS capping. First, CuS nanodots were fabricated as previously reported [36]. 2 mL of an aqueous $Na_2S \cdot 9H_2O$ solution (0.05 M) was added into 100 mL of an aqueous solution of $CuCl_2 \cdot 2H_2O$ (1 mM) and sodium citrate (0.68 mM). The mixture was reacted under stirring at room temperature for 5 min, after which the temperature was elevated to 80 °C for 15 min until a dark green suspension was obtained. The latter was immediately transferred to an ice bath.

HMSNs-SH (45 mg) were sonicated for 30 min in phosphate buffered saline (PBS, 50 mL, pH 7.4), before a solution of DOX (25 mg) in PBS (25 mL) was added and the mixture stirred in the dark for 24 h at room temperature. The product was centrifuged and washed with PBS

multiple times, resulting in DOX loaded NPs (HMSNs-DOX). The supernatants were all collected in order to determine the amount of drug loaded *via* ultraviolet (UV-vis) spectrophotometry (at 480 nm). Next, HMSNs-DOX and CS-SH (50 mg, 1:1 w/w) were dispersed in ultrapure water (100 mL) under magnetic stirring for 12 h, then subject to dialysis and freeze-drying to obtain HMSNs-CS-DOX. Finally, the resultant solid was dispersed in PBS (10 mL, 3 mg/mL) and a CuS dots suspension (10 mL, 1 mg/mL) added was to seal the pores on the surface of HMSNs. This mixture was stirred for 12 h at room temperature. The resultant product was centrifuged at 11,000 rpm for 15 min, washed with water three times, and dried at 60 °C under vacuum to obtain HMSNs-CS-DOX@CuS. The drug loading (DL) was quantified using UV-vis spectrophotometry (480 nm). The DL was calculated as follows:

$$DL = (DOX_a - DOX_b)/\text{total mass of NPs} \times 100\%$$

where DOX_a represents the total mass of DOX used in the preparation of the HMSNs-CS-DOX@CuS and DOX_b represents the un-encapsulated drug remaining in the supernatant.

2.3. Characterization

Transmission electron microscopy (TEM) was performed on a JEM 1200EX instrument (JOEL, Tokyo, Japan). Scanning electron microscopy (SEM) was undertaken with a Nova Nano microscope (FEI, Hillsboro, OR, USA). Fourier transform infrared (FT-IR) spectroscopy was performed with a Nicolet Nexus 670 spectrometer (Thermo Fisher, Waltham, MA, USA), and UV-vis spectra on a UV-3600 spectrophotometer (Shimadzu, Tokyo, Japan). Dynamic light scattering (DLS) and polydispersity index (PDI) data were collected on a BI-200SM instrument (Brookhaven Instruments, Holtsville, NY, USA). X-ray diffraction (XRD) patterns were measured using a D8 Advance X-ray powder diffractometer supplied with Cu Kα radiation (40 kV, 40 mA; Bruker, Billerica, MA, USA). N_2 adsorption/desorption isotherms were determined on a Tristar 3000 analyzer (Micromeritics, Atlanta, GA, USA), and the resultant data applied to measure the surface area and pore size of the obtained nanoparticles. X-ray photoelectron spectroscopy (XPS) was conducted with the aid of an Escalab 250Xi (ThermoFisher, Waltham, MA, USA).

2.4. Photothermal effects

In order to probe the photothermal conversion efficiency of the materials, aqueous suspensions of HMSNs-CS-DOX@CuS at different concentrations were irradiated using an 808

nm laser (1.0 W/cm^2). Experiments were also undertaken with varied laser power and a 1 mg/mL HMSNs-CS-DOX@CuS suspension. The thermal stability of HMSNs-CS-DOX@CuS was determined by irradiating for 5 min over five on-off cycles. In all cases, the temperature changes were recorded with an infrared thermal imaging system (FLIR A300, Shanghai Spectrum Electronics Technology Co., Shanghai, China). The volume of dispersion used for each experiment was 200 μL, and therefore the temperature of the suspension can be assumed to be constant throughout. The photothermal conversion efficiency (PTCE) was calculated using the equation [37, 38]:

$$\eta = hA(T_{max}-T_{am})-Q_0 \quad / \quad I(1-10^{-A_{808}})$$

where h and A represent the heat transfer coefficient and the surface area of the container respectively. T_{max} refers to the equilibrium temperature and T_{am} indicates the ambient temperature. Q_0 is the heat absorption of the quartz cell, I is the laser power density (250 mW), and A_{808} is the absorbency of the nanomaterials at 808 nm.

2.5. In vitro drug release

The release of DOX from HMSNs-CS-DOX@CuS was explored in PBS (pH 7.4), with or without the addition of 2 mM GSH or 10 mM GSH. In brief, a HMSNs-CS-DOX@CuS suspension (1 mg/mL) was loaded into a dialysis bag (molecular weight cutoff: 7000 Da) and dialyzed against PBS (25 mL, 37 °C) with shaking (150 rpm). Experiments were also performed with exposure to 808 nm laser irradiation (1.0 W/cm^2) for 10 min at selected time points (1, 6, 12, 24, and 36 h). At periodic time intervals, aliquots (1 mL) were removed and replaced with preheated fresh medium to maintain a constant volume. The concentration of DOX in the aliquots was measured using UV-vis spectrophotometry (480 nm) and used to calculate the cumulative release.

2.6. In vitro cytotoxicity study

MDA-MB-231 cells were cultured in DMEM supplemented with 10% v/v FBS, penicillin (100 U/mL), and streptomycin (100 μg/mL) ("complete DMEM"). HUVEC cells were employed as healthy control cells, and cultured using the same method above. ~1×10^4 cells in 150 μL medium were seeded in each well of a 96-well plate and incubated for 24 h at 37 ºC under 5% CO_2. 20 μL suspensions of the test formulations (free DOX, HMSNs-CS@CuS, and

HMSNs-CS-DOX@CuS) in PBS were added to the wells to give final concentrations of DOX ranging from 0.5 to 16 μg/mL, and blank PBS was employed as a control. After incubation for 24 h, where required the cells were illuminated by an 808 nm laser (1.0 W/cm^2) for 5 min. 20 μL of the MTT reagent (5 mg /mL in PBS) was then added to each well and the plate incubated for 4 h at 37 ℃ in the dark. The medium from each well was discarded and replaced by DMSO (200 μL). The optical densities of the samples were measured using a microplate reader (PowerWave XS, Bio-Tek, Winooski, VT, USA) at 490 nm. Three independent experiments were performed with five replicates in each.

Next, flow cytometry was employed to quantify apoptosis with Annexin V-FITC/PI staining. MDA-MB-231 cells (~10^5 cells in 2 mL complete DMEM) were seeded in six-well plates and incubated with NPs or free DOX for 12 h, with PBS used as a negative control. Cell apoptosis was performed using the Annexin V-FITC/PI kit. First, the treated cells were trypsinized and washed with cold PBS (pH 7.4). Next, Annexin V-FITC and PI were added in order according to the manufacturer's protocol. The cells were collected by centrifugation (1500 rpm, 10 min), and then resuspended in binding buffer (1 × 10^6 cells/mL). Flow cytometry was performed on a Accuri C6 instrument (Beckton-Dickson, Franklin Lakes, NJ, USA). Each experiment was repeated in triplicate, with three replicates in each experiment. The cell apoptosis profile was given by the ratio of Annexin V-FITC-positive cells PI-positive cells.

The calcein-AM/PI double-labeling method was used to further investigate the cytotoxicity of the HMSNs-CS-DOX@CuS system visually. MDA-MB-231 cells in complete DMEM were seeded into six-well plates (2 mL, ~10^5 cells/well) and cultured in an incubator for 24 h. The medium was then replaced by 2 mL of fresh medium containing different suspensions of the various formulations (at 50 μg/mL DOX concentration) was added. After being incubated for 4 h, each well was washed with PBS (1 mL) three times. Subsequently, the cells were stained with a mixed calcein-AM and PI solution for 15 min. Living (green) and apoptotic (red) cells were imaged under an inverted fluorescence microscope (TE-2000U, Nikon, Tokyo, Japan).

2.7. Confocal laser scanning microscopy (CLSM)

CLSM was used to demonstrate the uptake of HMSNs-CS-DOX@CuS in MDA-MB-231 cells. Cells were seeded in 24-well plates at a density of 1×10^5 cells per well (in 2 mL of medium) and cultured for 4 or 24 h at 37 ℃. A NP suspension in PBS and a free DOX solution a mixture of

DMSO and PBS (1:99 v/v) were prepared at 50 μg/mL DOX concentration. The medium was removed, 1 mL of each DOX-containing medium and fresh medium (1 mL) was added per well. After incubation for 2 h, the cells were washed with PBS (pH 7.4, 1 mL) and fixed with 500 μL of a 2.5% v/v aqueous glutaraldehyde solution for 10 min. The nuclei were stained with DAPI (50 μg/mL, 100 μL), and the cells examined by CLSM (FV1000 microscope, Olympus, Tokyo, Japan).

2.8. In vitro hemolysis assay

Pharmacological safety is a crucial factor to consider with any new medicine, and thus a hemolysis assay was performed to assess the suitability of HMSNs-CS-DOX@CuS for intravenous administration. Whole blood samples were obtained from SD rats, and red blood cells (RBCs) were isolated by centrifugation at 2000 rpm for 10 min. The collected RBCs were washed three times with cold saline, and then diluted into 10 mL of saline. Subsequently, free DOX, HMSNs-CS@CuS and HMSNs-CS-DOX@CuS were serially diluted to different concentrations and incubated with 0.2 mL of diluted RBC suspension for 3 h at 37 °C. Afterwards, all samples were centrifuged (1500 rpm, 15 min), and the supernatant was measured using a microplate reader (MULTSIKANMK3, Thermo Fisher, Waltham, MA, USA) at 540 nm. Negative (blank) and positive (100% hemolysis) control groups were obtained by mixing RBCs with PBS and deionized water, respectively. Each experiment was carried out in triplicate.

2.9. Blood circulation study

The blood circulation profile of DOX-containing NPs was measured using healthy SD rats (*n* = 3), and all animal experiments were performed in accordance with a protocol approved by the Animal Care and Use Committee of Kunming Medical University. The rats were intravenously injected with PBS solutions/suspensions of free DOX or HMSNs-CS-DOX@CuS (7.5 mg DOX equiv. kg^{-1}) through the tail vein. At predetermined time points (0.5, 1, 2, 3, 4, 8, 12, 16, 20 and 24 h) post-injection, 15 μL of blood was collected from the ocular vein. The blood samples were centrifuged at 3000 rpm for 15 min and 4 ºC, and the concentration of DOX in the blood was measured by UV-vis spectrophotometry as reported previously [39].

2.10. In vivo biodistribution

The drug release and distribution behavior of HMSNs-CS-DOX@CuS *in vivo* were studied using a Maestro™ *in vivo* imaging system (CRi Inc.,Woburn, MA, USA). The model fluorescent

molecule DIR was incorporated in the NPs in place of DOX (giving HMSNs-CS-DIR@CuS). HMSNs-CS-DIR@CuS NPs were synthesized using the same procedure as for the DOX-loaded analogue (see Section 2.2), but with DIR replacing DOX in the reactions. A tumor-bearing mouse model was created by injecting 100 μL of a MDA-MB-231 cell suspension (containing ~5×10^6 MDA-MB-231 cells) subcutaneously into the right flank area of nude mice. Tumor-bearing mice were randomly divided into two groups (8 in each). When the volume of the tumors reached approximately 100 mm^3 (calculated as $L \times M^2/2$; L: tumor length, M: tumor width), HMSNs-CS-DIR@CuS or free DIR were intravenously injected through the tail vein. Fluorescence scans were performed at periodic time intervals (1, 4, 8, 12 and 24 h) after injection. After *in vivo* imaging, the mice were sacrificed by carbon dioxide asphyxiation and the tumor, heart, liver, spleen, lungs and kidneys were excised, washed with cold saline, and imaged *ex vivo* on the Maestro system [40, 41].

2.11. In vivo PA imaging

In vivo PA imaging was performed on a multi-mode ultrasound/PA imaging system (Visual Sonics Inc. NY, USA). 100 μL of a PBS suspension of HMSNs-CS-DOX@CuS ([CuS] = 10 mM) was intravenously injected into tumor-bearing nude mice (generated as detailed in Section 2.10). PA images were collected before and at various time points after injection.

2.12. In vivo antitumor efficacy

Tumor-bearing mice (generated as detailed in Section 2.10) were randomly divided into 5 groups (8 in each). When the tumor volume reached ca. 100 mm^3, the mice were given intravenous injections of saline (control), free DOX, HMSNs-CS@CuS+NIR, HMSNs-CS-DOX@CuS and HMSNs-CS-DOX@CuS+NIR (7 mg/kg of DOX equiv.) through the tail vein every other day for 30 days. The body weight and tumor size were monitored every other day during the treatment period, and the survival curve evaluated by Kaplan-Meier analysis [38]. At the end of the experiment, the mice were sacrificed and the tumors excised and photographed. The tumors of mice in NIR treatment groups were irradiated with the 808 nm NIR laser (1.0 W/cm^2) for 10 min every second day (at 24 h post-injection).

2.13. Blood biochemical indices

On 15 day of the treatment in Section 2.12, 5 mice from each group were selected randomly, and a 200 μL blood sample was collected from each mouse through the tail vein after fasting

overnight. All the obtained blood samples were subjected to analysis on an automated AU5400 biochemistry analyzer (Olympus, Tokyo, Japan), and the concentrations of liver function indicators [aspartate aminotransferase (AST) and alanine aminotransferase (ALT)] and renal function indicators [creatinine (CRE) and urea nitrogen (BUN)] were determined. All procedures complied with the manufacturer's instructions.

2.14. Histological analyses

The tumor tissue and other major organs were removed from one mouse in each group 30 days post-treatment and fixed in 4 % formaldehyde for 48 h. Paraffin sections were prepared for histological analysis including H&E and TUNEL staining, followed by observation by light microscopy.

2.15. Statistical analysis

Statistical analysis was conducted using the Student's T test for comparison of two groups and one-way ANOVA for multiple groups, the latter followed by a Newman-Keuls test if $P < 0.05$. * denotes $P < 0.05$, ** $P < 0.01$ and *** $P < 0.001$.

3. Results and discussion

3.1. Preparation and characterization of HMSNs-CS-DOX@CuS

The FT-IR spectra (Supplementary Information, Fig. S1) and zeta potential changes (Fig. 1A) verified the successful synthesis of HMSNs-CS nanocomposites. As can be seen in Fig. S1, the spectrum of the composite HMSNs-CS (green line) displays characteristic signals of all components, including the absorption bands at 1019 cm^{-1} and 1027 cm^{-1} for the hydroxyl groups of CS, as well as the stretching vibration at 790 cm^{-1} (Si-O) of HMSNs. Moreover, the successful synthesis of HMSNs-CS was confirmed by the disappearance of the CS-NH_2 peak at 1569 cm^{-1}. In addition, the zeta potential of the HMSNs displayed a significant increase from −48.5 mV to −19.6 mV after the introduction of CS, as shown in Fig. 1A. This is expected since CS is a cationic polymer containing abundant amine groups. Both sulfhydrylation modification and negatively charged CuS decreased the surface potential of HMSNs in the synthetic process, and the introduction of positive potential CS resulted in the slightly negative potential of final HMSNs-CS-DOX@CuS.

To generate DOX loaded NPs, the DOX was loaded into the core of HMSNs before the CS

grafting and CuS capping (see Fig. S2 for a photograph of the particles after DOX loading). UV–vis absorption spectra of HMSNs-CS-DOX@CuS (Fig. S3) display the characteristic absorbance peaks of DOX (e.g. at 480 nm), indicating that DOX was successfully loaded into the formulation. The DL of DOX was calculated to be 46.1% (w/w). This DL is comparable with previously reported HMSNs-based drug delivery systems [42]. CuS nanodots were then capped onto the surface of HMSNs-CS-DOX (giving HMSNs-CS-DOX@CuS) to act as gatekeepers, and further improve the dispersity and stability. It can be seen from the mean hydrodynamic size measurement (Fig. 1B) that modification with CS increased the size of the HMSNs. After the surface incorporation of CuS dots, the hydrodynamic size decreased slightly. The mean hydrodynamic size of HMSNs-CS-DOX@CuS NPs measured by DLS was 150 ± 13 nm with a relatively narrow dispersity (PDI: 0.15). N_2 adsorption/desorption isothermals of HMSNs and HMSNs-CS-DOX@CuS are shown in Fig. S4A. It can be observed that HMSNs exhibit a typical mesoporous structure. After loading with DOX and capping with CuS, the pore size of HMSNs (4.48 nm) was decreased to 1.84 nm in the HMSNs-CS-DOX@CuS system (Fig. S4B), further demonstrating the efficient capping of CuS into the pores. The stability of HMSNs-CS-DOX@CuS NPs in several biorelevant media (e. g. PBS, DMEM culture medium and a cell culture medium containing 10% FBS (FBS/ DMEM)) was studied by DLS measurements, and data reveal the NPs to maintain a constant size in all the environments explored (Fig. S5). Agglomeration of drug-loaded NPs was not observed even after incubation for 7 days in PBS, DMEM or FBS/DMEM, which confirms the long-term stability of HMSNs-CS-DOX@CuS.

Successful modification with the CuS gatekeeper was verified by XRD and XPS. The HMSNs XRD pattern (Fig.1C) exhibits only a broad feature centered at around 22°, typical of SiO_2 [27]. There are additional characteristic Bragg reflections at 33.6° and 46.2° in the pattern of HMSNs-CS-DOX@CuS (Fig. 1D), which can be assigned to the (200) and (220) reflections of CuS [43]. XPS was utilized to study the valence states of Cu and S in the nanocomposites (Fig. 1E and F). The spectrum of the HMSNs-CS shows the peaks expected due to the presence of Si and O in the material, as well as a C 1s signal (Fig. 1E). HMSNs-CS-DOX@CuS presents characteristic S 2p and Cu 2p peaks (Fig. 1F), as well as bands arising from C, Si, and O. These results all verified that CuS nanodots were successfully decorated onto the surface of HMSNs-CS-DOX.

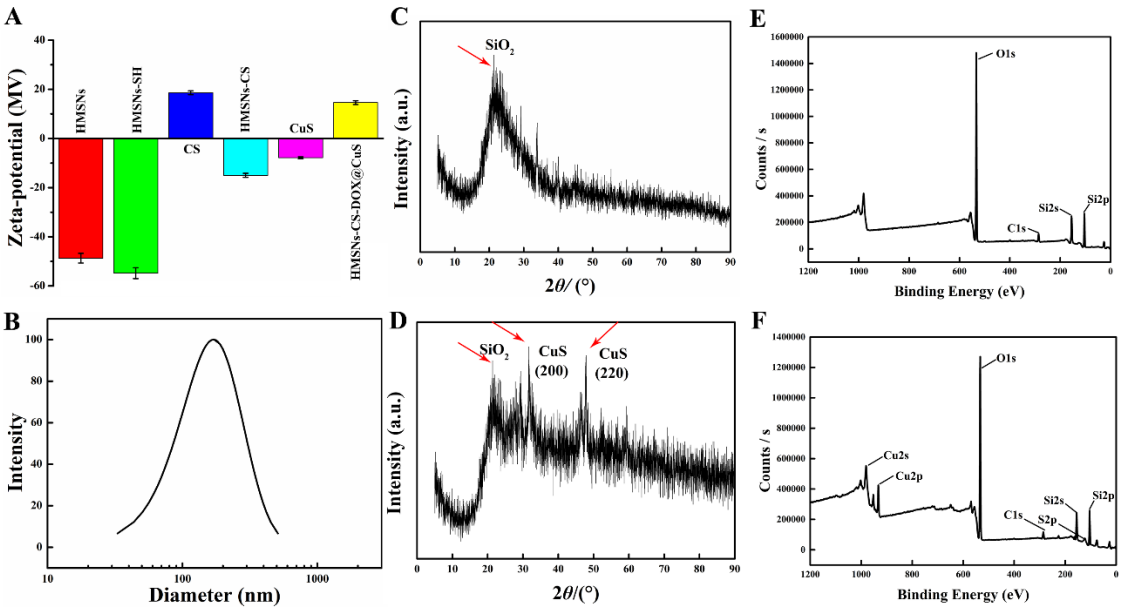

Fig. 1. Characterizing data on the nanomaterials, showing: (A) zeta potentials; (B) DLS data for HMSNs-CS-DOX@CuS; XRD patterns of (C) HMSNs and (D) HMSNs-CS-DOX@CuS; XPS spectra of (E) HMSNs-CS and (F) HMSNs-CS-DOX@CuS.

The morphology of the materials was characterized by TEM and SEM. TEM images (Fig. 2A) show that the as-prepared HMSNs have hollow spherical structures with uniform size of approximately 130 nm, which is confirmed by SEM (Fig. 2B). As shown in Fig. 2C, the CuS quantum dots have a size of around 5-10 nm. At the end of the synthetic process (Fig. 2D), it can be seen that CS is wrapped around the HMSNs and CuS is present at the particle surfaces (red arrows). The HMSNs-CS-DOX@CuS retain the spherical shape of the HMSNs starting material. Given the size of the pores in the HMSMs (ca. 4.5 nm) and the size of the CuS quantum dots (ca. 5-10 nm), it appears that the CuS quantum dots are retained at the surface of the HMSNs. However, it should be noted that some penetration of the dots into the pores cannot be ruled out from the analytical data.

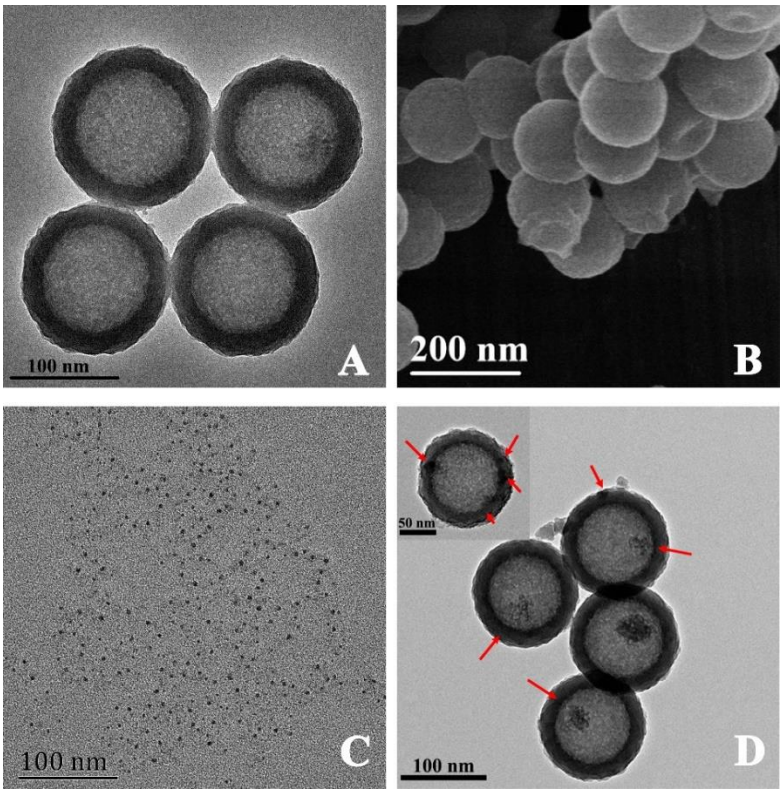

Fig. 2. Electron microscopy images. (A) TEM and (B) SEM images of HMSNs. (C) TEM image of CuS nanodots. (D) TEM image of HMSNs-CS-DOX@CuS. Red arrows indicate the CuS nanodots on the HMSNs surfaces.

3.2. In vitro GSH/NIR-triggered drug release.

DOX release from HMSNs-CS-DOX@CuS was explored *in vitro* under different conditions. As shown in Fig. 3, without the addition of GSH only 19 % of the DOX cargo is released at pH 7.4 after 48 h, while the introduction of NIR can increase the cumulative release of DOX to 29.5% after 48 h. The cumulative release of DOX from HMSNs-CS-DOX@CuS reaches about 33% after 48 h in the presence of 2mM GSH and exposure to NIR irradiation, but if the concentration of GSH is increased to 10 mM the extent of release after 48 h is elevated to *ca.* 71%. We can see that in the absence of NIR exposure there is reduced DOX release, at both GSH concentrations explored. These observations arise because the CuS NPs act as a gatekeeper to the surface pores in the HMSNs. The CuS NPs are connected to the surface by a disulfide bond which can be easily cleaved under high concentrations of GSH, leading to accelerated release of DOX with higher GSH concentrations. Exposure to NIR laser irradiation causes the temperature to rise by dint of the PTT properties of CuS. This increases the energy of the system, accelerating the rate of S-S bond breaking and the extent of pore opening at the HMSN surface. The interactions between DOX and the HMSNs are also likely to become weakened with a rise in temperature, further

accelerating drug release.

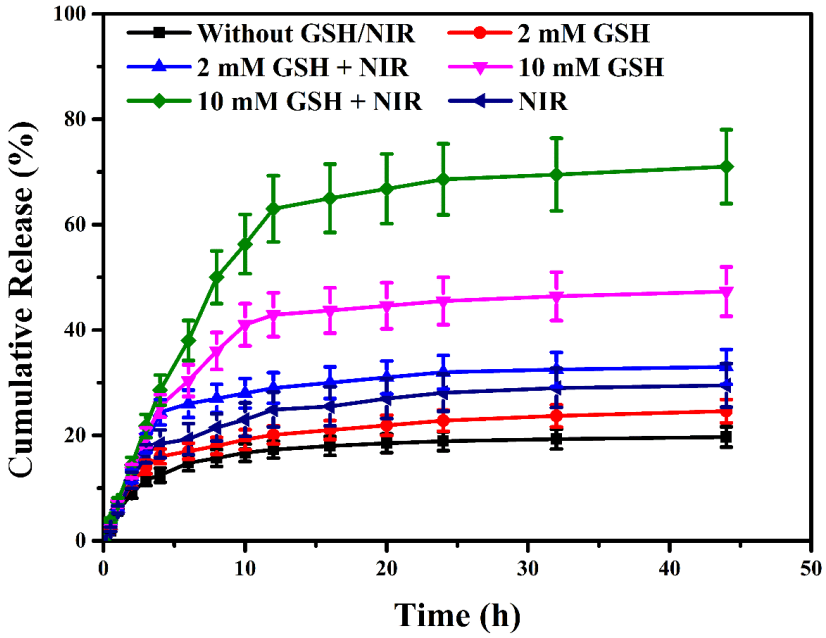

Fig. 3. *In vitro* DOX release in PBS at different GSH concentrations, with or without 808 nm laser irradiation (1 W/cm^2), measured with a dialysis method (n = 3, mean ± S.D.).

3.3. In vitro photothermal properties

We next investigated the photothermal properties of HMSNs-CS-DOX@CuS *in vitro*, on account of the strong absorption of CuS in the NIR region. First, different concentrations of the HMSNs-CS-DOX@CuS solutions were irradiated with a 1.0 W/cm^2 808 nm laser, and the temperature changes were recorded in real time. As shown in Fig. S6A, the temperature of a HMSNs-CS-DOX@CuS aqueous dispersion increased rapidly upon laser irradiation. Higher concentrations of NPs result in greater temperature increases. When the concentration of the HMSNs-CS-DOX@CuS was 1.0 mg/mL, the temperature reaches 57 °C after laser irradiation for 5 min. In contrast, the water negative control group shows only a very small temperature change under the same conditions. In addition, laser power-dependent photothermal behavior can be clearly seen in Fig. S6B. The PTCE (η) of HMSNs-CS-DOX@CuS was calculated to be 36.4 %, which is comparable to that of similar PTT agents reported in the literature [21]. Moreover, the NPs displayed negligible loss of performance over five 1.0 W/cm^2 laser irradiation on/off cycles (see Fig. S6C), indicating the photostability of HMSNs-CS-DOX@CuS. Taken together, all these observations imply that the HMSNs-CS-DOX@CuS nanomaterial can be used as a potential photothermal agent and for NIR-mediated ablation of tumors.

3.4. In vitro cytotoxicity

The effect of chemotherapy and photothermal therapy on cell proliferation was evaluated *in vitro* using the MTT assay. Firstly, healthy HUVEC cells were used to assess if the nanocarriers themselves have any cytotoxicity. As indicated in Fig. 4A, HMSNs-CS@CuS showed negligible cytotoxicity to normal HUVEC cells in the concentration range explored (> 95 % cell viability), confirming that the HMSNs-CS@CuS possesses excellent cytocompatibility. The blank carrier is also non-toxic to MDA-MB-231 cells (Fig. 4B). All of the other formulations cause concentration-dependent reductions in the viability of both HUVEC and MDA-MB-231 cells (Fig. 4A, B). Compared to the other groups, the proliferation of the cells was significantly reduced after treatment with HMSNs-CS-DOX@CuS NPs and NIR irradiation.

Flow cytometry was further carried out to analyze the extent of apoptosis in the different treatment groups, and the extent of cell death was calculated as the sum percentage of the upper left quadrant (representing late-stage apoptosis), lower right quadrant (early apoptosis) and right upper quadrant (necrosis). As presented in Fig. 4C, HMSNs-CS-DOX@CuS+NIR (33.0 ± 5.8 %) treatment significantly increased the death of MDA-MB-231 cells over HMSNs-CS@CuS+NIR (23.0 ± 3.1 %), free DOX (18.2 ± 2.1 %), HMSNs-CS-DOX@CuS (24.2 ± 3.2 %) and the negative control (1.4 ± 0.8 %). The results indicate that apoptosis arises from the synergistic combination of both chemotherapy and PTT [38, 44, 45]. The composite NPs prepared in this work display a comparable cytotoxic effect against breast cancer cells to previously reported HMSNs loaded with DOX [43, 46]. However, when NIR irradiation was applied, the HMSNs-CS-DOX@CuS NPs showed a significantly stronger effect, which may be attributed to the combination chemo-PTT therapy. These results are verified using calcein-AM/PI double staining after the different treatments (Fig. 4D). Cells treated with HMSNs-CS-DOX@CuS and NIR displayed very strong red fluorescence, indicating dead cells. With the other treatments there are some dead cells visible, but markedly fewer than after combined chemo/PTT therapy. All these results indicated that the HMSNs-CS-DOX@CuS NPs can effectively combine PTT and chemotherapy in a multifunctional drug delivery system.

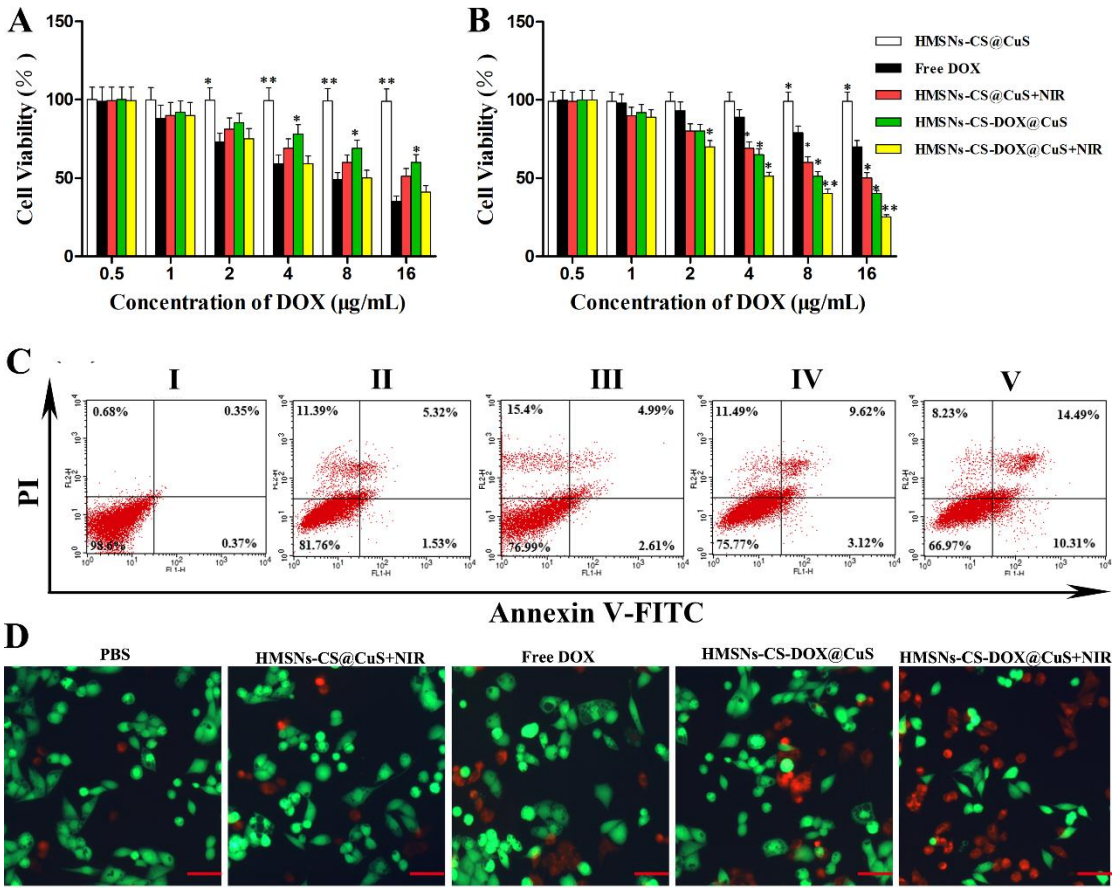

Fig. 4. Relative viabilities of (A) HUVEC and (B) MDA-MB-231 cells incubated with the different formulations at various DOX concentrations. (C) Flow cytometry results for Annexin V-FITC and PI co-stained MDA-MB-231 cells. (I) Negative control, (II) free DOX, (III) HMSNs-CS@CuS + NIR, (IV) HMSNs-CS-DOX@CuS, (V) HMSNs-CS-DOX@CuS + NIR. (D) Fluorescence images of calcein-AM (green)/PI (red) double stained cells (scale bars = 50 μm). Apoptotic cells are stained red. $^{*}P < 0.05$, $^{**}P < 0.01$ compared with the free DOX group.

3.5. In vitro cellular uptake

MDA-MB-231 human breast cancer cells were used to study *in vitro* cellular uptake of the NPs. Cells were cultivated with free DOX or HMSNs-CS-DOX@CuS for 4 h or 24 h, and then observed by CLSM (Fig. 5). The fluorescence of cells incubated with HMSNs-CS-DOX@CuS was notably higher than those cultured with free DOX at both timepoints studied. HMSNs-CS-DOX@CuS uptake after 24 h was markedly higher than at 4 h. The main reason for this is that the NPs enter the cells *via* the EPR effect [47, 48], and the tumor environment-responsive nanocarrier facilitates the release of DOX. These findings are consistent with previous work showing that HMSNs increased drug uptake through NPs endocytosis and

accumulation inside cells [44].

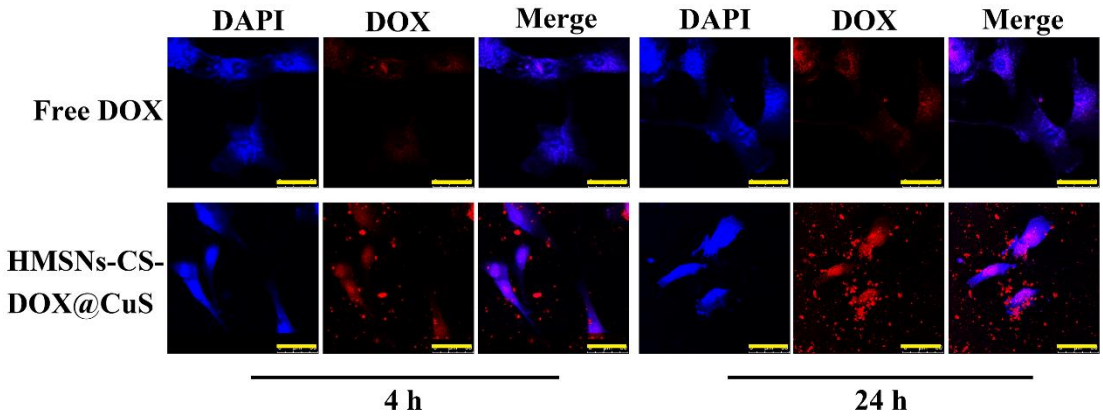

Fig. 5. (A) CLSM data depicting cellular uptake of DOX by MDA-MB-231 cells at 4 h or 24 h (all scale bars = 50 μm).

3.6. Hemocompatibility and pharmacokinetics

Before the developed nanomaterials can be applied *in vivo*, biosafety must be considered. The effect of free DOX, HMSNs-CS@CuS and HMSNs-CS-DOX@CuS on the hemolytic behavior of RBCs was thus investigated (Fig. S7). The results reveal that free DOX induced severe RBC lysis even at very low concentrations, whereas negligible hemolysis was detected with HMSNs-CS@CuS and HMSNs-CS@CuS. The NPs thus have good biocompatibility and should be safe for intravenous application. The hemolysis caused by the HMSNs-CS-DOX@CuS NPs was less than 10% even at a concentration of 250 μg/mL.

The *in vivo* pharmacokinetics of free DOX and HMSNs-CS-DOX@CuS NPs were evaluated in SD rats. As can be seen in Fig. S8, owing to their size and surface modification, the blood circulation time of HMSNs-CS-DOX@CuS *in vivo* is much longer than that of free DOX. 4 h after injection of free DOX, the concentration of DOX in the plasma had declined to an undetectable level, while DOX from the HMSNs-CS-DOX@CuS NPs can be detected in the blood more than 24 h post-injection.

3.7. In vivo photothermal conversion and biodistribution

MDA-MB-231 tumor-bearing mice injected with HMSNs-CS-DOX@CuS or PBS were exposed to an 808 nm NIR laser (1.0 W/cm^2) for 5 min. Real-time images were recorded using an IR thermal camera (Fig. 6A). The temperature at the tumor site increased by about 26 ℃ (from 28 to 54 ℃) in the presence of HMSNs-CS-DOX@CuS (Fig. 6B). However, there was minimal

change in the temperature of the control group (PBS + NIR, Fig. 6B). This is because HMSNs-CS-DOX@CuS has strong NIR absorption properties and a high PTCE at 808 nm.

In order to evaluate the real-time uptake of the HMSNs-CS-DOX@CuS *in vivo*, the MDA-MB-231 tumor bearing mice were injected with HMSNs-CS-DIR@CuS or free DIR (control) and imaged using an *in vivo* fluorescence imaging system (Fig. 6C). The images of the HMSNs-CS-DIR@CuS treated animals show that the fluorescence gradually concentrated at the tumor site over time, and the fluorescence was still visible at 24 h. From 1 h, the tumor sites exhibited a higher fluorescence signal than the other organs, and clear NP accumulation at the tumor site was observed after 8 h. In the DIR control group, there is fairly strong fluorescence at the liver and tumor site after 1 h, but the fluorescence at tumor had almost disappeared after 8 h. This arises because of the rapid excretion of DIR in solution, whereas the NPs can accumulate at the tumor site.

To further explore the biodistribution of HMSNs-CS-DIR@CuS, mice were sacrificed 24 h post-injection, and the heart, liver, spleen, lung, kidney, and tumor were excised and imaged *ex vivo* (Fig. 6D). After 24 h, the HMSNs-CS-DIR@CuS NPs were concentrated in the tumor site, with the liver also showing fluorescence but nothing visible in the other organs. In contrast, the free DIR was almost all located in the liver. This is because DIR is hydrophobic, and thus is trafficked to the liver for onward metabolism [49]. The fluorescence intensity of HMSNs-CS-DIR@CuS at the tumor site was approximately 2.5-fold higher than that of free DIR (Fig. 6E). The fluorescence intensity in the organs is higher for the free DIR group than the HMSNs-CS-DIR@CuS group.

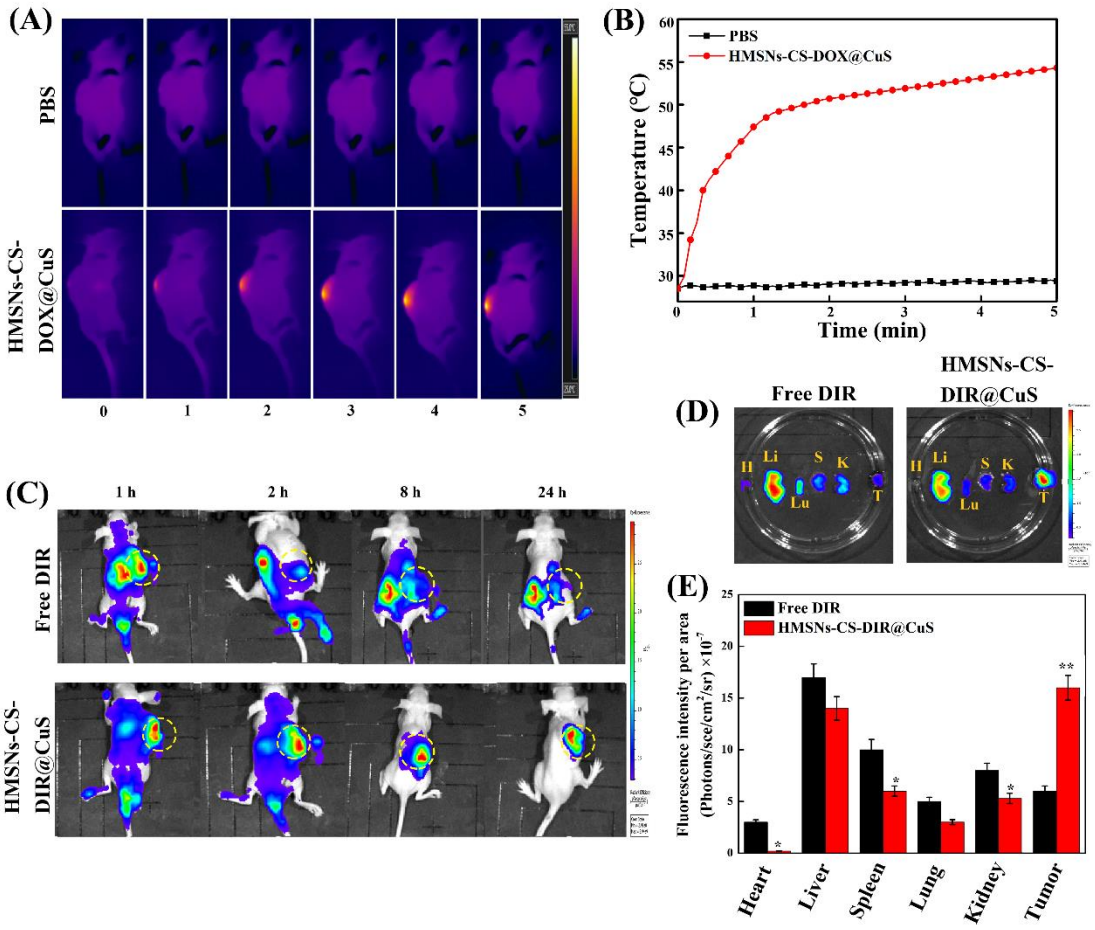

Fig. 6. (A) Thermal images and (B) the corresponding tumor temperature changes of MDA-MB-231 tumor-bearing mice after treatment with PBS or HMSNs-CS-DOX@CuS with 808 nm laser irradiation at 1.0 W /cm^2 for 5 min. (C) *In vivo* fluorescence images of MDA-MB-231 xenograft nude mice after i.v. injection of free DIR and HMSNs-CS-DIR@CuS (images taken from different mice; yellow dotted circles indicate the tumor sites). (D) *Ex vivo* images showing the fluorescence intensity in the different organs after 24 h showing the heart (H), liver (Li), spleen (S), lungs (Lu), kidney (K) and tumor (T). (E) statistical analysis of the data in (D) (n = 8, results are shown as mean ± S.D.). * P < 0.05 and ** P < 0.01 compared with the free DIR group.

3.8. In vivo PA imaging

PA imaging is a newly developed method, based on the photoacoustic effect, for deep tissue penetration [50]. It can be used to monitor the accumulation and distribution of NPs in tumors [51]. The possibility of PA imaging using the HMSNs-CS-DOX@CuS NPs was evaluated *in vivo*. A US image was taken as a contrast background to confirm the location of the tumor before i.v. injection of HMSNs-CS-DOX@CuS NPs. It can be seen in Fig. 7 that there is a distinct PA signal at the tumor site in MDA-MB-231 tumor-bearing nude mice after treatment with of

HMSNs-CS-DOX@CuS, with the maximum signal detected at 12 h post-injection. The results suggested that the HMSNs-CS-DOX@CuS NPs may be used as a PA imaging contrast agent for imaging-guided cancer treatment.

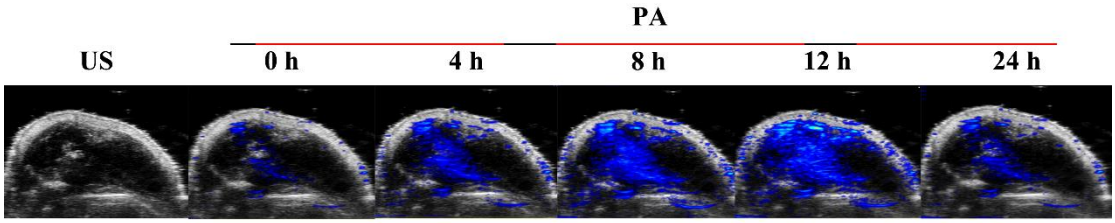

Fig. 7. US (0 h) and PA images of MDA-MB-231 tumor-bearing mice before and at various time points after i.v. injection of HMSNs-CS-DOX@CuS NPs, the tumor model was created by injecting MDA-MB-231 cell suspension subcutaneously into the right flank area of nude mice.

3.9. In vivo therapeutic efficacy and safety evaluation

The anticancer efficacy and safety of HMSNs-CS-DOX@CuS NPs were investigated using MDA-MB-231 tumor-bearing mice. With most treatment groups, the tumor volume increased steadily with time (Fig. 8A), with the greatest rise noted with the negative control group. However, when mice were given HMSNs-CS-DOX@CuS+NIR there was a clear decline in tumor volume, and the final volume of the tumor excised at day 30 was 38 ± 5 mm^3 (Fig. 8A, B), significantly lower than with the saline group (2200 ± 115 mm^3). The weight of the mice was recorded every other day throughout the treatment period to study any potential tissue toxicity of the NPs (Fig. 8C). Mice treated with free DOX show a gradual decrease in body weight, suggesting that DOX had serious side effects, in agreement with previously published literature [52, 53]. The body weights increased to different degrees after the mice were given saline, HMSNs-CS@CuS+NIR, HMSNs-CS-DOX@CuS and HMSNs-CS-DOX@CuS+NIR treatments. The saline treated mice gained most weight, presumably because of tumor growth. The HMSNs-CS-DOX@CuS+NIR treatment showed essentially no increase in body weight throughout the experiment, consistent with the NPs being biocompatible and the synergistic chemo/PTT therapy virtually eradicating the tumor. The other treatments led to some increase in weight, likely to be a result of tumor growth.

Survival curves for the mice were calculated using the Kaplan-Meier method (Fig. 8D). Mice treated with HMSNs-CS-DOX@CuS + NIR had a 60% survival rate after 60 days. However, the mice treated with saline all died within 34 days. The other treatments extended lifetimes over the control, but nevertheless all the mice were dead within 58 days. It can be seen that the combined

chemo-PTT combined treatment can prolong the survival times of mice to a much greater extent than single therapy approaches.

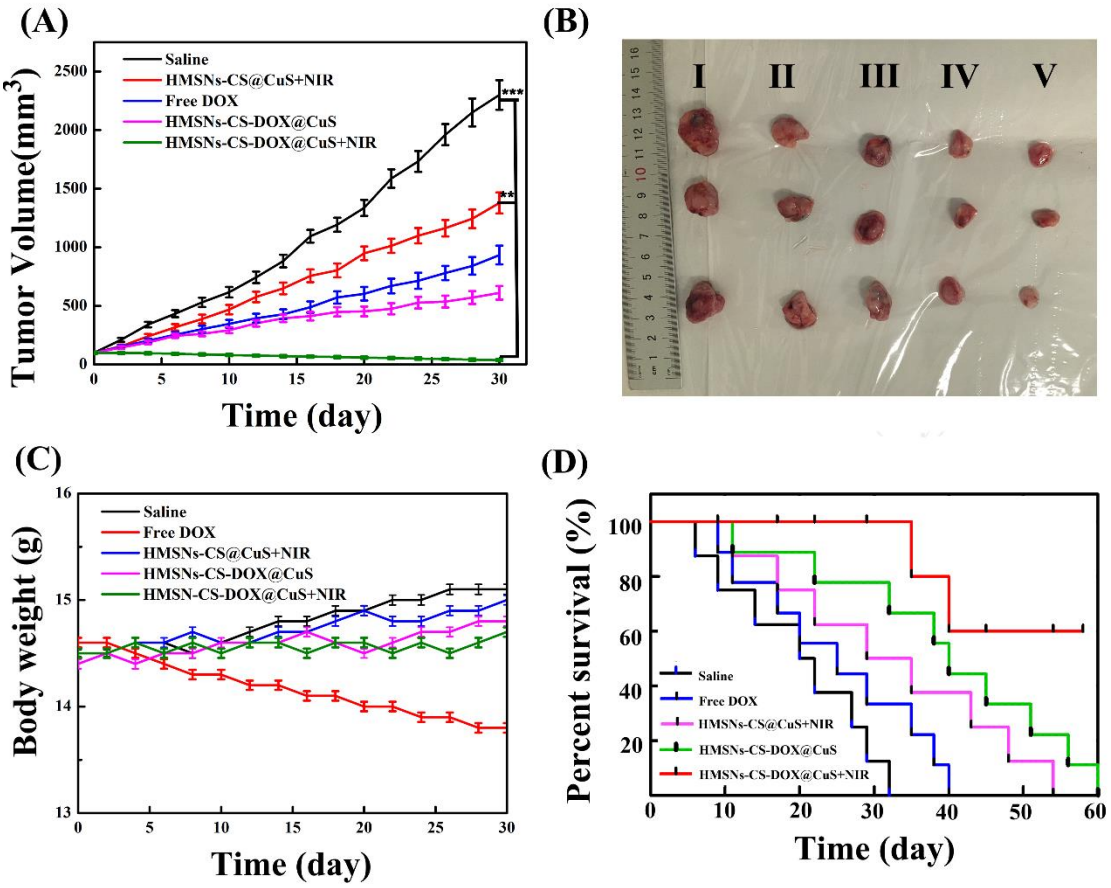

Fig.8. *In vivo* tumor model data. (A) Real-time measurements of tumor volume. ***P*< 0.01, and ****P*< 0.001 compared to the saline control. (B) Representative photos of tumor tissues resected after 30 days of treatment with (I) saline (control), (II) free DOX, (III) HMSNs-CS@CuS+NIR, (IV) HMSNs-CS-DOX@CuS, (V) HMSNs-CS-DOX@CuS+NIR. (C) Mean body weights as a function of time. (D) Kaplan-Meier survival curves.

In general, the HMSNs-CS-DOX@CuS NPs appear to have good biocompatibility and can reduce the toxic side effects of DOX. This was explored in more detail by assaying blood markers including liver function (AST and ALT) and kidney function indexes (CRE and BUN). The results in Fig. S9 show elevated levels of all markers in the free DOX group (denoting serious hepatic and renal injury), but there are no significant differences between mice treated with saline, HMSNs-CS@CuS and HMSNs-CS-DOX@CuS. This indicates there is no negative impact or toxicity caused by the NPs during treatment.

3.10. Ex vivo analyses

The major organs (heart, liver, spleen, lung, kidney) and tumor were harvested and H&E

stained at the end of the 30 days treatment period. As shown in Fig. 9A, the free DOX group results in some damage to the liver (mild hepatocellular cystic steatosis and local inflammation), but no damage was observed with the other organs. For all other treatments, the H&E slices are indistinguishable from the negative control for all organs except in the case of the kidneys, which results from the renal toxicity due to the metabolism of free DOX. Turning to the tumor tissue, severe necrosis can be seen in mice treated with HMSNs-CS-DOX@CuS+NIR, (Fig. 9B). Much reduced necrosis to is observed after the other treatments. TUNEL analysis was additionally performed (Fig. 9B). TUNEL slices showed there was no apoptosis in the tumors of the control group, but widespread apoptosis of tumor cells (brown cells) is visible for animals treated with HMSNs-CS-DOX@CuS+NIR. Quantitative analyses of the TUNEL data are given in Fig. 9C. The percentage of apoptotic cells after treatment with HMSNs-CS-DOX@CuS+NIR (82 ± 7%) was higher than HMSNs-CS-DOX@CuS (64 ± 5%) and HMSNs-CS@CuS+NIR (49 ± 4%). All data demonstrate the effectiveness of the combined chemo-PTT treatment in the *in vivo* model of breast cancer.

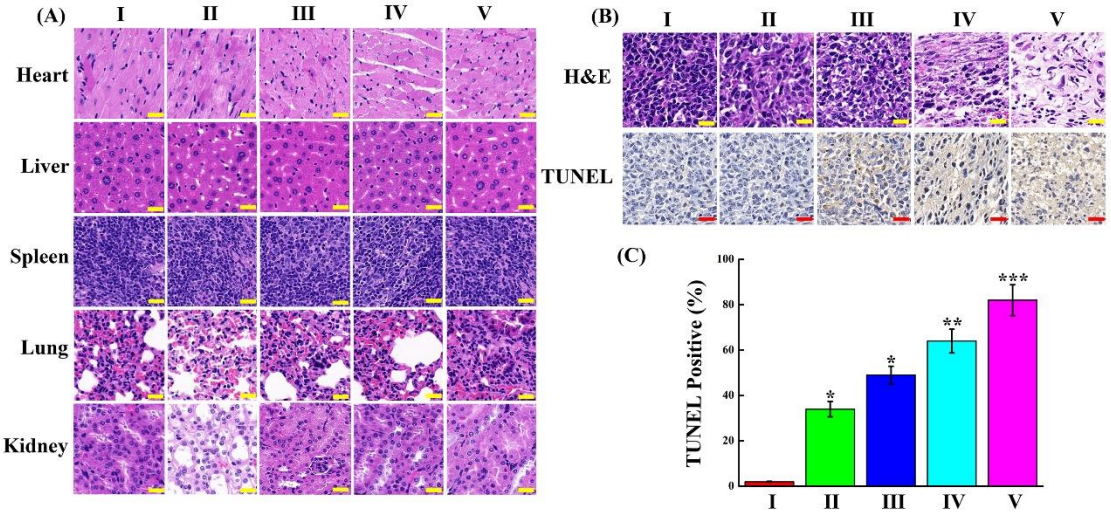

Fig. 9. Histopathology data. (A) Sections of the heart, liver, spleen, lung and kidney stained with hematoxylin and eosin. (B) H&E and TUNEL stained tumor sections. Scale bars: 50 μm. (C) Quantitative analysis of the TUNEL positive rates (n = 5, results shown as mean ± S.D.), * P< 0.05, ** P < 0.01, ***P< 0.001 compared with saline. Groups are as follows: (I) saline (control), (II) free DOX, (III) HMSNs-CS@CuS+NIR, (IV) HMSNs-CS-DOX@CuS, (V) HMSNs-CS-DOX@CuS+NIR.

4. Conclusions

A multifunctional nanotheranostic platform (HMSNs-CS-DOX@CuS) was prepared in this work, based on HMSNs. This has a high drug loading capacity for DOX (46.1 % w/w), and targets drug release to the tumor microenvironment. This targeted delivery is achieved through the attachment (*via* S-S bonds) of CuS nanodots as gatekeepers at the surface pores of the HMSNs. When exposed to NIR laser irradiation, the HMSNs-CS-DOX@CuS generate energy, causing S-S bond breaking and accelerating drug release. In addition, these photothermal properties of the composite render it suitable for photothermal therapy. The NPs possess a uniform size distribution (150 ± 13 nm), good water dispersibility, and can be easily taken up by breast cancer cells. *In vitro* experiments show that the blank NPs were nontoxic, but the DOX loaded systems are able to induce cell death. A systematic *in vitro* and *in vivo* evaluation confirmed the HMSNs-CS-DOX@CuS platform to give highly effective synergistic chemo-PTT therapy and have trackable thermal/photoacoustic dual-imaging properties. This work may open up a new avenue for NIR-enhanced synergistic therapy with simultaneous multimodal imaging.

Acknowledgements

This research was financially supported by grant 16410723700 from the Science and Technology Commission of Shanghai Municipality, the Scientific Research Foundation of Yunnan Provincial Department of Education (2021J0228), the Yunnan Provincial Department of Science and Technology-Kunming Medical University Joint Project on Applied Basic Research (2018FE001(-162)), and the National Natural Science Foundation of China (81460647).

References

[1] S. Niu, G.R. Williams, J. Wu, J. Wu, X. Zhang, H. Zheng, S. Li, L.-M. Zhu, A novel chitosan-based nanomedicine for multi-drug resistant breast cancer therapy, Chem. Eng. J. 369 (2019) 134-149.

[2] S.S. Feng, C. Shu, Chemotherapeutic engineering: Application and further development of chemical engineering principles for chemotherapy of cancer and other diseases, Chem. Eng. Sci. 58 (2003) 4087-4114.

[3] J. Wei, Z. Huiyuan, W. Jilian, Z. Guangxi, L. Zhonghao, L. Yuxia, G. Sanjay, CuS@MOF-based well-designed quercetin delivery system for chemo-photothermal therapy, ACS Appl. Mater. Inter. 10 (2018) 34513-34523.

[4] Z. Tian, X. Yao, K. Ma, X. Niu, J. Grothe, Q. Xu, L. Liu, S. Kaskel, Y. Zhu, Metal–organic framework/graphene quantum dot nanoparticles used for synergistic chemo- and photothermal therapy, ACS Omega 2 (2017) 1249-1258.

[5] X. Yao, X. Niu, K. Ma, P. Huang, J. Grothe, S. Kaskel, Y. Zhu, Graphene quantum dots-capped magnetic mesoporous silica nanoparticles as a multifunctional platform for controlled drug delivery, magnetic hyperthermia, and photothermal therapy, Small 13 (2017) 1602225.

[6] J. Wu, D.H. Bremner, S. Niu, M. Shi, L. Zhu, Chemodrug-gated biodegradable hollow mesoporous organosilica nanotheranostics for multimodal imaging-guided low-temperature photothermal therapy/chemotherapy of cancer, ACS Appl. Mater. Inter. 10 (2018) 42115-42126.

[7] X. Li, J. Shan, W. Zhang, S. Su, L. Yuwen, L. Wang, Recent advances in synthesis and biomedical applications of two-dimensional transition metal dichalcogenide nanosheets, Small 13 (2017) 1602660.

[8] L. Du, H. Qin, T. Ma, T. Zhang, D. Xing, In vivo imaging-guided photothermal/photoacoustic synergistic therapy with bioorthogonal metabolic glycoengineering-activated tumor targeting nanoparticles, ACS Nano 11 (2017) 8930-8943.

[9] Z. Zhang, J. Wang, C. Chen, Near-infrared light-mediated nanoplatforms for cancer thermo-chemotherapy and optical imaging, Adv. Mater. 25 (2013) 3869-3880.

[10] Y. Wang, K. Wang, R. Zhang, X. Liu, X. Yan, J. Wang, E. Wagner, R. Huang, Synthesis of core–shell graphitic carbon@silica nanospheres with dual-ordered mesopores for cancer-targeted photothermochemotherapy, ACS Nano 8 (2014) 7870-7879.

[11] Q.-L. Li, D. Wang, Y. Cui, Z. Fan, L. Ren, D. Li, J. Yu, AIEgen-functionalized mesoporous silica gated by cyclodextrin-modified CuS for cell imaging and chemo-photothermal cancer therapy, ACS Appl. Mater. Inter. 10 (2018) 12155-12163.

[12] S. Goel, F. Chen, W. Cai, Synthesis and biomedical applications of copper sulfide nanoparticles: from sensors to theranostics, Small 10 (2014) 631-645.

[13] L. Xiangmei, Y. Tianshe, H. Yifan, Z. Liang, Y. Huiran, J. Jiayang, L. Shujuan, Z. Qiang, H. Wei, In situ growth of CuS/SiO-based multifunctional nanotherapeutic agents for combined photodynamic/photothermal cancer therapy, ACS Appl. Mater. Inter. 10 (2018) 31008-31018.

[14] L. Ren, X. Liu, Q. Wang, L. Zhang, G. Deng, F. Zhou, J. Lu, Facile fabrication of a magnetically smart PTX-loaded Cys–Fe_3O_4/CuS@BSA nano-drug for imaging-guided chemo-photothermal therapy, Dalton T. 46 (2017) 2204-2213.

[15] R.K. Kankala, H. Zhang, C. Liu, K.R. Kanubaddi, C. Lee, S. Wang, W. Cui, Hélder A. Santos, K. Lin, A. Chen, Metal species–encapsulated mesoporous silica nanoparticles: current advancements and latest breakthroughs, Adv. Funct. Mater. 29 (2019) 1902652.

[16] R.K. Kankala, Y. Han, J. Na, C. Lee, Z. Sun, S. Wang, T. Kimura, Y.S. Ok, Y. Yamauchi, A. Chen,

K C.W. Wu, Nanoarchitectured structure and surface biofunctionality of mesoporous silica nanoparticles, Adv. Mater. 32 (2020) 1907035.

[17] N. Mojgan, M. Marzieh, A. Khalil, T.S. Mohammad, R. Mohammad, A. Mona, Fabrication of acetylated carboxymethylcellulose coated hollow mesoporous silica hybrid nanoparticles for nucleolin targeted delivery to colon adenocarcinoma, Carbohyd. Polym. 197 (2018) 157-166.

[18] G. Tao, W. He, Y. Wang, F. Yu, J. Ge, W. Yang, Dispersity, mesoporous structure and particle size modulation of hollow mesoporous silica nanoparticles with excellent adsorption performance, Dalton T. 47 (2018) 13345-13352.

[19] J. Wen, K. Yang, F. Liu, H. Li, Y. Xu, S. Sun, Diverse gatekeepers for mesoporous silica nanoparticle based drug delivery systems, Chem. Soc. Rev. 46 (2017) 6024-6045.

[20] Q.-L. Li, Y. Sun, Y.-L. Sun, J. Wen, Y. Zhou, Q.-M. Bing, L.D. Isaacs, Y. Jin, H. Gao, Y.-W. Yang, Mesoporous silica nanoparticles coated by layer-by-layer self-assembly using cucurbit[7]uril for *in vitro* and *in vivo* anticancer drug release, Chem. Mater. 26 (2014) 6418-6431.

[21] C. Zhang, W. Sun, Y. Wang, F. Xu, J. Qu, J. Xia, M. Shen, X. Shi, Gd-/CuS-loaded functional nanogels for MR/PA imaging-guided tumor-targeted photothermal therapy, ACS Appl. Mater. Inter. 12 (2020) 9107-9117.

[22] S. Liang, X. Deng, Y. Chang, C. Sun, S. Shao, Z. Xie, X. Xiao, P. Ma, H. Zhang, Z. Cheng, J. Lin, Intelligent hollow Pt-CuS janus architecture for synergistic catalysis-enhanced sonodynamic and photothermal cancer therapy, Nano Lett. 19 (2019) 4134-4145.

[23] X. Li, M. Bottini, L. Zhang, S. Zhang, J. Chen, T. Zhang, L. Liu, N. Rosato, X. Ma, X. Shi, Y. Wu, W. Guo, X.J. Liang, Core-satellite nanomedicines for in vivo real-time monitoring of enzyme-activatable drug release by fluorescence and photoacoustic dual-modal imaging, ACS Nano 13 (2019) 176-186.

[24] S. Niu, G.R. Williams, J. Wu, J. Wu, X. Zhang, X. Chen, S. Li, J. Jiao, L.M. Zhu, A chitosan-based cascade-responsive drug delivery system for triple-negative breast cancer therapy, J. Nanobiotecg. 17 (2019) 95.

[25] T. Wang, D. Wang, H. Yu, M. Wang, J. Liu, B. Feng, F. Zhou, Q. Yin, Z. Zhang, Y. Huang, Intracellularly acid-switchable multifunctional micelles for combinational photo/chemotherapy of the drug resistant tumor, ACS Nano 10 (2016) 3496-3508.

[26] M. Xuan, J. Shao, Z. Jie, L. Qi, L. Dai, Magnetic Mesoporous Silica Nanoparticles Cloaked by Red Blood Cell Membranes: Applications in Cancer Therapy, Angew. Chem. Int. Ed. 130 (2018) 6157-6161.

[27] J. Wu, D.H. Bremner, S. Niu, D. Li, R. Tang, L.M. Zhu, Multifunctional A7R peptide-modified hollow mesoporous Silica@Ag_2S nanotheranostics for photoacoustic/near-infrared fluorescence imaging-guided tumor-targeted chemo-photothermal therapy, J. Biomed. Nanotechnol. 15 (2019) 1415-1431.

[28] C. Liu, Y. Han, R.K. Kankala, S. Wang, A. Chen, Subcellular performance of nanoparticles in cancer therapy, Int. J. Nanomed. 15 (2020) 675-704.

[29] H. Yang, C. Tang, C. Yin, Estrone-modified pH-sensitive glycol chitosan nanoparticles for drug delivery in breast cancer, Acta Biomater. 73 (2018) 400-411.

[30] S. Niu, D.H. Bremner, J. Wu, J. Wu, H. Wang, H. Li, Q. Qian, H. Zheng, L. Zhu, L-peptide functionalized dual-responsive nanoparticles for controlled Paclitaxel release and enhanced apoptosis in breast cancer cells, Drug Deliv. 25 (2018) 1275-1288.

[31] J.Y. Lee, U. Termsarasab, M.Y. Lee, D.H. Kim, S.Y. Lee, J.S. Kim, H.J. Cho, D.D. Kim,

Chemosensitizing indomethacin-conjugated chitosan oligosaccharide nanoparticles for tumor-targeted drug delivery, Acta Biomater. 57 (2017) 262-273.

[32] R.K. Kankalaa, C. Liu, D. Yang, S. Wang, A. Chen, Ultrasmall platinum nanoparticles enable deep tumor penetration and synergistic therapeutic abilities through free radical species-assisted catalysis to combat cancer multidrug resistance, Chem. Eng. J. 383 (2020) 123138.

[33] X. He, M. Ding, J. Li, H. Tan, Q. Fu, L. Li, Biodegradable multiblock polyurethane micelles with tunable reduction-sensitivity for on-demand intracellular drug delivery, Rsc Adv. 4 (2014) 24736-24746.

[34] D. Zhao, J. Wu, C. Li, H. Zhang, Z. Li, Y. Luan, Precise ratiometric loading of PTX and DOX based on redox-sensitive mixed micelles for cancer therapy, Colloids Surface B 155 (2017) 51-60.

[35] W. Ke, W. Yin, Z. Zha, J.F. Mukerabigwi, W. Chen, Y. Wang, C. He, Z. Ge, A robust strategy for preparation of sequential stimuli-responsive block copolymer prodrugs via thiolactone chemistry to overcome multiple anticancer drug delivery barriers, Biomaterials 154 (2018) 261-274.

[36] N. Lu, W. Fan, X. Yi, S. Wang, Z. Wang, R. Tian, O. Jacobson, Y. Liu, B.C. Yung, G. Zhang, Z. Teng, K. Yang, M. Zhang, G. Niu, G. Lu, X. Chen, Biodegradable hollow mesoporous organosilica nanotheranostics for mild hyperthermia-induced bubble-enhanced oxygen-sensitized radiotherapy, ACS Nano 12 (2018) 1580-1591.

[37] J. Wu, D.H. Bremner, S. Niu, H. Wu, J. Wu, H. Wang, H. Li, L.-M. Zhu, Functionalized MoS_2 nanosheet-capped periodic mesoporous organosilicas as a multifunctional platform for synergistic targeted chemo-photothermal therapy, Chem. Eng. J. 342 (2018) 90-102.

[38] Y. Li, J. Wu, G.R. Williams, S. Niu, J. Zhou, Y. Yang, X. Zhang, Z. Fu, D. Li, L.-M. Zhu, Synergistic chemo-photothermal suppression of cancer by melanin decorated MoOx nanosheets, ACS Appl. Bio Mater. 2 (2019) 4356-4366.

[39] Y. Zhong, M. Dimde, D. Stobener, F. Meng, C. Deng, Z. Zhong, R. Haag, Micelles with sheddable dendritic polyglycerol sulfate shells show extraordinary tumor targetability and chemotherapy *in vivo*, ACS Appl. Mater. Inter. 8 (2016) 27530-27538.

[40] F. Gao, J. Wu, S. Niu, T. Sun, F. Li, Y. Bai, L. Jin, L. Lin, Q. Shi, L.-M. Zhu, L. Du, Biodegradable, pH-sensitive hollow mesoporous organosilica nanoparticle (HMON) with controlled release of pirfenidone and ultrasound-target-microbubble-destruction (UTMD) for pancreatic cancer treatment, Theranostics 9 (2019) 6002-6018.

[41] X. Zhang, S. Niu, G.R. Williams, J. Wu, X. Chen, H. Zheng, L.M. Zhu, Dual-responsive nanoparticles based on chitosan for enhanced breast cancer therapy, Carbohyd. Polym. 221 (2019) 84-93.

[42] K. Cheng, Y. Zhang, Y. Li, Z. Gao, F. Chen, K. Sun, P. An, C. Sun, Y. Jiang, B. Sun, A novel pH-responsive hollow mesoporous silica nanoparticle (HMSN) system encapsulating doxorubicin (DOX) and glucose oxidase (GOX) for potential cancer treatment, J. Mater. Chem. B, 7 (2019) 3291-3302.

[43] X. Meng, Z. Liu, Y. Cao, W. Dai, K. Zhang, H. Dong, X. Feng, X. Zhang, Fabricating aptamer-conjugated PEGylated-MoS_2/$Cu_{1.8}S$ theranostic nanoplatform for multiplexed imaging diagnosis and chemo-photothermal therapy of cancer, Adv. Funct. Mater. 27 (2017) 1605592.

[44] Y. Zhang, W. Xiu, Y. Sun, D. Zhu, Q. Zhang, L. Yuwen, L. Weng, Z. Teng, L. Wang, RGD-QD-MoS_2 nanosheets for targeted fluorescent imaging and photothermal therapy of cancer, Nanoscale 9 (2017) 15835-15845.

[45] J. Nam, S. Son, L.J. Ochyl, K. Rui, A. Schwendeman, J.J. Moon, Chemo-photothermal therapy

combination elicits anti-tumor immunity against advanced metastatic cancer, Nat. Commun. 9 (2018) 1074.

[46] S.P. Hadipour Moghaddam, M. Yazdimamaghani, H. Ghandehari, Glutathione-sensitive hollow mesoporous silica nanoparticles for controlled drug delivery, J. Control. Release 282 (2018) 62-75.

[47] Y. Wang, F. Wang, Y. Liu, S. Xu, Y. Shen, N. Feng, S. Guo, Glutathione detonated and pH responsive nano-clusters of Au nanorods with a high dose of DOX for treatment of multidrug resistant cancer, Acta Biomater. 75 (2018) 334-345.

[48] X. Tao, J. Gou, Q. Zhang, X. Tan, T. Ren, Q. Yao, B. Tian, L. Kou, L. Zhang, X. Tang, Synergistic breast tumor cell killing achieved by intracellular co-delivery of doxorubicin and disulfiram via core-shell-corona nanoparticles, Biomater. Sci. 6 (2018) 1869-1881.

[49] S. Tang, Q. Meng, H. Sun, J. Su, Q. Yin, Z. Zhang, H. Yu, L. Chen, Y. Chen, W. Gu, Y. Li, Tumor-microenvironment-adaptive nanoparticles codeliver paclitaxel and siRNA to inhibit growth and lung metastasis of breast cancer, Adv. Funct. Mater. 26 (2016) 6033-6046.

[50] T. Liu, S. Shi, C. Liang, S. Shen, L. Cheng, C. Wang, X. Song, S. Goel, T.E. Barnhart, W. Cai, Z. Liu, Iron oxide decorated MoS_2 nanosheets with double PEGylation for chelator-free radiolabeling and multimodal imaging guided photothermal therapy, ACS Nano 9 (2015) 950-960.

[51] L. Chen, X. Zhou, W. Nie, W. Feng, Q. Zhang, W. Wang, Y. Zhang, Z. Chen, P. Huang, C. He, Marriage of albumin-gadolinium complexes and MoS_2 nanoflakes as cancer theranostics for dual-modality magnetic resonance/photoacoustic imaging and photothermal therapy, ACS Appl. Mater. Inter. 9 (2017) 17786-17798.

[52] E. Li, Y. Yang, G. Hao, X. Yi, S. Zhang, Y. Pan, B. Xing, M. Gao, Multifunctional magnetic mesoporous silica nanoagents for in vivo enzyme-responsive drug delivery and MR imaging, Nanotheranostics 2 (2018) 233-242.

[53] X. Liu, C. Wang, H. Ma, F. Yu, F. Hu, H. Yuan, Water-responsive hybrid nanoparticles codelivering ICG and DOX effectively treat breast cancer via hyperthermia-aided DOX functionality and drug penetration, Adv. Healthc. Mater. 8 (2019) 1801486.